Experimental Investigations of Heat-Flux and Temperature Predictions by New Inverse Technique

MUSTAFA B. AL-HADITHI[1], ABDULHASSAN A. KARAMALLA[2]
[1]Chemical and Petrochemical Engineering Department,
College of Engineering, University of Anbar,
Anbar, IRAQ
[2]Mechanical Engineering Department, University of Technology,
Baghdad, IRAQ

Abstract:- This paper describes the developed method for predictions of transient internal surface temperatures and heat-flux obtained from thermocouples, which are installed through the wall of the rocket motor nozzle. Heat-Flux was estimated by using the prediction of internal surface temperatures from numerical solutions of the inverse heat conduction problem (IHCP). Three Heat-Flux gauges are manufactured and used in convergent, throat, and divergent sections. The temperatures are measured with starting operation of the rocket motor along the gauges where the thermocouples are connected to the data acquisition system interfacing with the PC. The measured unsteady temperature behavior is approximated by polynomials third degree in space and time. The measurement results indicate that the maximum reading temperatures are at the throat section. No differences in time were appearing in curves to reach maximum prediction surface temperatures.

Keywords:- Heat Conduction, Numerical Solution, Thermocouples, Data Acquisition, rocket Motor Nozzle, Heat-Flux Gauge, Inverse Heat Conduction problem.

Received: May 22, 2022. Revised: October 24, 2022. Accepted: November 26, 2022. Published: December 31, 2022.

1 Introduction

The determination of the temperature distribution in a rocket nozzle wall requires knowledge of the total heat transferred from combustion gases. It is important to estimate accurately the heat transfer to the wall in order to achieve an optimum thermal insulation system. In heat transfer studies, many experimental difficulties may be arising in implanting Heat-Flux sensors or thermocouples at the surface for heat transfer measurements. Furthermore, the presence of a probe at the surface disturbs the condition of the boundary and the flow process adjacent to it, and thus actual wall heat flux. It is therefore important to estimate accurately the convective heat transfer to the wall in order to achieve an optimum thermal protection system. In these circumstances, it is therefore desirable to predict the surface temperature and heat flux is accomplished by inverting the measured temperature by thermocouples which are located interior to the surface of the solid material. Such a problem is termed the inverse heat conduction problem. The design of the Heat-Flux gauge shown in Figure 1 provides a thermal insulating air space around the rod and at the end of the rod. This type of design is called herein a "single active surface Heat-Flux gauge" compared with that in [1]. The (IHCP) can recover the unknown parameters such as surface temperatures, coefficient heat transfer, heat flux, material thermos-physical parameters, internal heat sources, and boundary geometry by measuring the temperature history information at the boundaries or at some points inside the heat transfer system, [2], [3], [4], [5], [6]. The physical problem involves a convective heat slab of finite thickness having a heat sink at one surface and perfect insulation at the other. These circumstances provide a one-dimensional analysis of the problem. A new method to measure thermal contact conductance is introduced by [7] with a time-dependent temperature field of the surfaces of two bodies in contact recorded with an infrared thermography camera. The resulting temperature data are the input for the solution of the related inverse heat conduction problem and yield the boundary heat flux at the contact interface. The effectiveness of the inverse modeling technique in [8] is associated with the accuracy of the temperature data input into the model which was obtained using a new measurement and analysis technique incorporating infra-red probes and thermocouple arrays that accurately determine both casting and die surface temperatures. Also, the measurement methods and

analysis techniques presented a powerful illustration of the application of an inverse heat transfer modeling technique to a materials engineering application enabling the determination of the most accurate heat transfer coefficient and heat flux data. From [9] we find the inverse method was proved to be robust and can be used to retrieve accurately the temperature-dependent effective thermal conductivity by retrieving the input parameters from numerically generated transient temperature profile, the retrieved
results increased nonlinearly with increasing temperature and gas pressure, the values fell within 0.014–0.044 W/(m_K) for the temperature range of 280–1080 K and gas pressure range of 0.01 Pa to 100 kPa. The retrieved effective thermal conductivities were validated by comparing the results with those measured from a steady-state method. In [10], the authors solved the two-dimensional transient heat transfer where the FDM is adopted to solve the direct problem without an internal heat source and the model predictive control method is used to solve the inverse problem. Besides, the residual principle is introduced to optimize the regularization parameter during the inversion process, thereby improving the efficiency of inversion in terms of speed and time, it demonstrates that the proposed methods have higher accuracy in the inversion process.
In the inverse problem, the heat flux is unknown at x = 0 but temperature readings at x=L are given from the sensor and are denoted by TM(L,t), utilizing the measured data, unknown heat flux is estimated. In our study using FDM and the tridiagonal system of equations with the Thomas algorithm technique are used to solve the problem numerically. The study of the inverse problem using the first type boundary condition is estimated by iteration method in conjunction with the measured temperature history at the interior of the copper rod can be considered at the other end and the problem can be considered as a one-dimensional unsteady heat conduction system.

2 The Inverse Problem

The estimation of surface temperature and heat-flux are obtained by an iterative scheme that can be used to obtain these values from the measured temperature history at three locations by embedded thermocouples inside the material copper rod. A one-dimensional heat conduction equation can be achieved by using implicit representation at the interior nodes as in [11]

$$(T_i^{n+1} - T_i^n) / \Delta t = \alpha (T_{i-1}^{n+1} - 2 T_i^{n+1} + T_{i+1}^{n+1}) / \Delta x^2 \quad (1)$$

With the following initial and boundary conditions,

$$T(x,0) = TI \text{ for } 0< x < L \text{ and } t=0$$

$$T(x1,t) = TM1(t) \text{ for } x=x1 \text{ and } t > 0 \quad (2)$$
$$T(x2,t) = TM2(t) \text{ for } x=x2 \text{ and } t > 0$$
$$T(x3,t) = TM3(t) \text{ for } x=x3 \text{ and } t > 0$$

Where TM1, TM2 and TM3 are the measured temperatures by thermocouples at each location along the rod of gauge. These locations are given by x1, x2, and x3, and TI is the initial temperature of the material. The heat conduction equation can be obtained with implicit representation at the surface where x=0 as follows,

$$(q_0'' / \Delta x k) - (T_0^{n+1} - T_1^{n+1}) / \Delta x^2 = (T_0^{n+1} - T_0^n) /(2\alpha\Delta t) \quad (3)$$

Where the subscripts 0 and 1 denote the node identifiers and the superscript (n+1) indicates that the value is taken at the time (t+Δt). The solution of equation (1) can be obtained by solving the tridiagonal system of equations with the Thomas algorithm given by [12]

$$- s T_{i-1}^{n+1} + (1+2s) T_i^{n+1} - s T_{i+1}^{n+1} = T_i^n \quad (4)$$

For $0 < x < L$ and $t > 0$
Where $s = \alpha \Delta t / \Delta x^2$

Rearranging equation (3) into tridiagonal form as

$$[- 2 - \Delta x^2 /(\alpha\Delta t)] T_0^{n+1} + 2 T_1^{n+1} = - (2 q_0'' \Delta x / k) - (\Delta x^2 / (\alpha\Delta t)) T_0^n \quad (5)$$

For $x = 0$ and $t > 0$

In the foregoing equations (4) and (5), T_0 and q_0'' is unknown parameters, thus the solution of the complete problem from x = 0 to x = x1 where the location of thermocouple cannot be obtained readily because the boundary condition is not known at x = 0. But when an interior temperature history is given at x1, then, the estimating of internal surface temperatures (T_0) and heat fluxes (q_0'') can be obtained with iteration techniques.

2.1 The Iterative Procedure

The iteration scheme begins with two arbitrary values of internal surface temperature (T_{01}) and

(T_{02}). The numerical solution of equation (4) gives T (T_{01}) and T (T_{02}) at x = x1. The solution is tested at each T_0 for convergence with the measured temperatures (TM) as boundary conditions by,

$$ABS\ (T^{i}(x,t) - T^{i-1}(x,t)) \leq 10^{-5} \quad (6)$$

Where $T^{i}(x,t)$ is the calculated temperature in time (t) and location (x) with current iteration (i). The new value of T_0 is obtained by linear interpolation as in [13] with the using shooting method or (method de tire), if the solution diverges at this boundary condition a new value of temperature (T_{ON}) can be obtained from two arbitrary values of T(T_{01}) and T(T_{02}) at the given (T_{01}) and (T_{02}) which is known as new surface temperature (T_{ON}) as follows,

$$T_{ON} = [(TM - T(T_{01}))* T_{02} - (TM - T(T_{02}))* T_{01})] / (T(T_{02}) - T(T_{01})) \quad (7)$$

The iteration continues until the convergence is reached at the measured boundary conditions. A computer program has been constructed using the above procedure to predict all the surface temperatures and heat fluxes with time by Eq's (4&5). The measured temperatures field TM are read by the program through the approximated polynomials of the third degree in space and time.

3 Temperature Measuring Equipment

3.1 Heat-Flux Gauge

Figure 1 shows a detailed engineering drawing of the Heat-Flux gauge used. High conductivity copper rod as shown in Figure1.a with (80 mm) in length and (6mm) in diameter are instrumented with three fine rapid-response cromel-alumel k-type thermocouples (TC1, TC2, and TC3) thermocouple balls are brazed into small holes drilled into the rod surface and integrated into one Heat-Flux gauge. The thermocouples are attached at distances of (8,16, and 32 mm) from the gas side surface, copper sleeve is positioned around the copper rod as shown in Figure1.b and soldered to the rod at its right end. The (1mm) gap between the rod and sleeve prevents heat conduction from the neighboring wall to the rod, so that the assumption of one-dimensional heat flow along the rod is justified. To avoid pulling the thermocouple wires from their position, they are set in place in the copper fitting with epoxy cement as shown in Figure1.c. The assembled Heat-Flux gauge shown in Figure 1.d is inserted into the cavities in the nozzle wall and sealed with a rubber ring washer, (5) bolts type (M 8 X 1.25) are used to connect each Heat-Flux gauge with nozzle wall cavity.

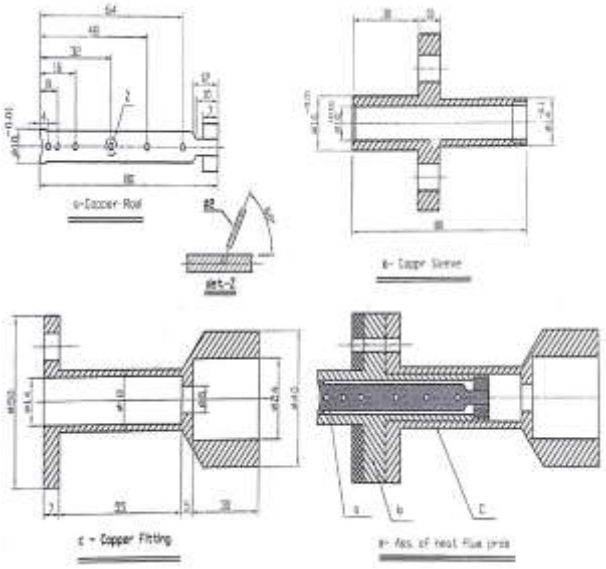

Fig. 1: Heat-Flux Gauge

3.2 Data Acquisition and Processing System

Figure 2 shows the diagram of an automated data acquisition and processing system. The system permits (30) thermocouple k-type to be used as inputs to amplifiers compensation circuit type (AD594 / AD595). Two multiplexers are used to select the inputs from the amplifiers and process it through a single analog-to-digital converter ADC type (ADC0804) as in [14].

Typically, the multiplexers are used to sample across more than one input. The ADC samples one channel switches to the next channel, samples it, switches to the next channel, samples it, and so on. Because the ADC is sampling many channels instead of one, the sampling rate must be considered as applied to the sum of the channels. If the sampling rate is 100 ks/s and there are 30 channels, then the sampling rate for one of the channels is 100/30 =3.33 ks/s. Software is used in automated data acquisition and instrument control systems.

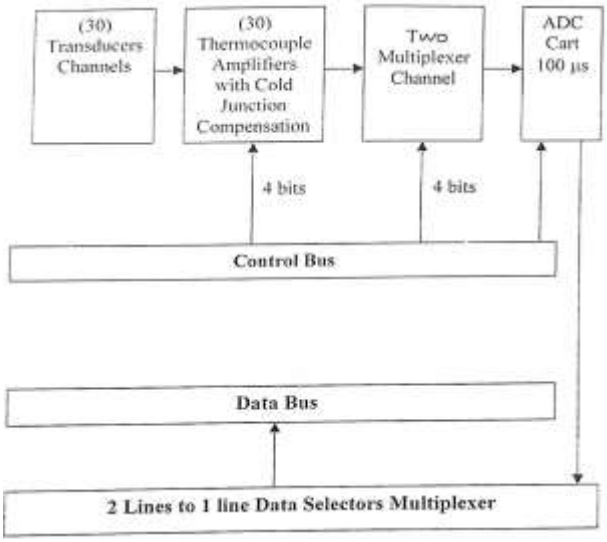

Fig. 2: Components of Data Acquisition System

3.3 Time Constant and Calibrations of Thermocoupl

No instrument responds instantly to a change in its environment. Thus in a region where the temperature is changing, a thermocouple will not be at the temperature of its environment and, hence, cannot indicate the true temperature. As in [15] gives the methods of thermocouple changes with the environments. The interval between the time when the environment reaches a given temperature and the time when the sensor element indicates this temperature is called the time constant. A nomograph for the calculation of time constant (τ_1) appears in Figure 3 given by [16]. From this figure, the first turning line has been graduated to give directly the value of the platinum time constant wire at NACA standard sea-level conditions. The time constant for a wire of any other material can be obtained from the above figure. According to the procedure used in Figure 3, and with thermocouple k-type (nickel-10% chromium, +, versus nickel-5% aluminum, -,) in the present work of 0.25 mm in diameter. The calculated time constant is (0.00145 s). The sensor was calibrated with a standard thermocouple reader model Goery M4011 for two reference temperatures. The thermocouple was calibrated against freezing water temperature and together against pure chloroform liquid with a boiling point of (61.2 ˚C). An error of (±0.5 ˚C) was observed. The limits of error for the common letter designated thermocouples types are given by [15] which are taken from American Standard ANSI.

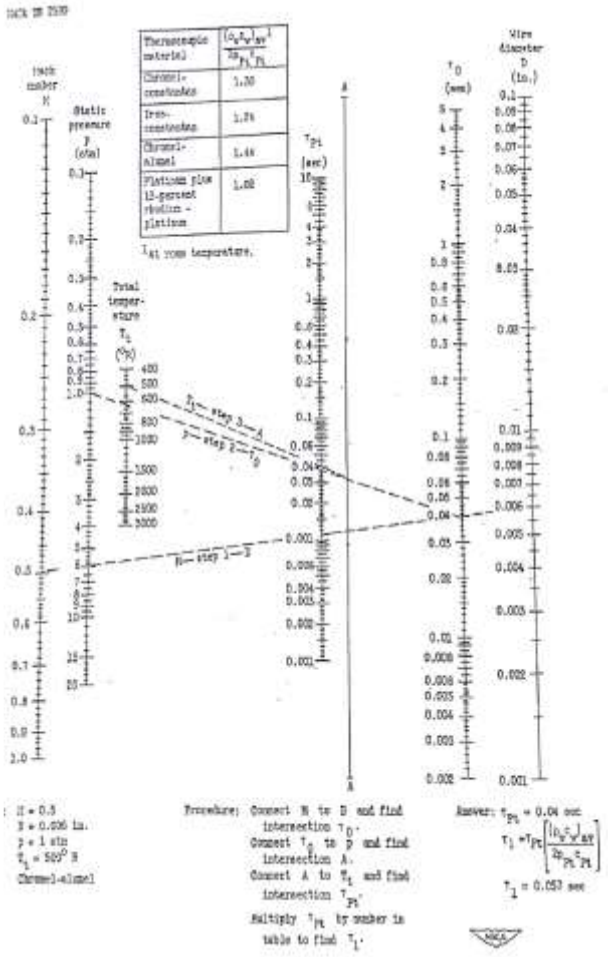

Fig. 3: Nomograph for Computing τ_1 From [16]

4 Experimental Executions

Three Heat-Flux gauges are manufactured and used in the convergent, throat and divergent sections (No.1, No.2, and No.3) respectively, these gauges are tested individually before using in their nozzle locations. A successful experimental test is running with grain configuration and complete assembly of the rocket motor given in Figure 4, the throat diameter is (15 mm).

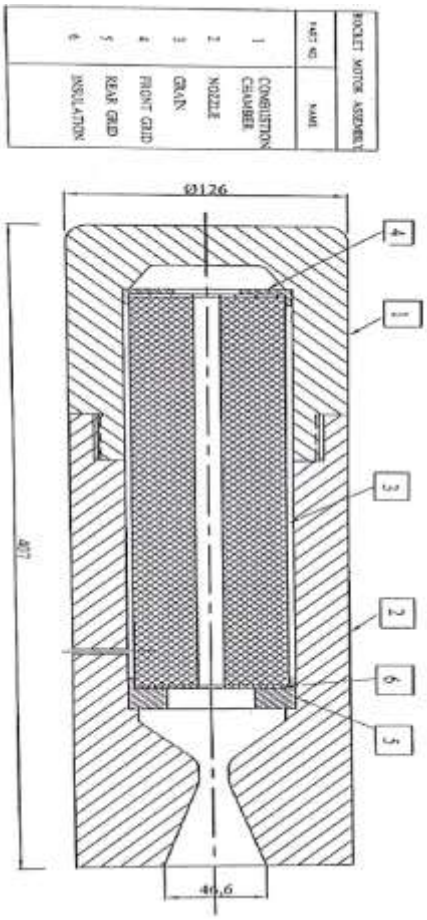

Fig. 4: Experimental Rocket Motor Assembly

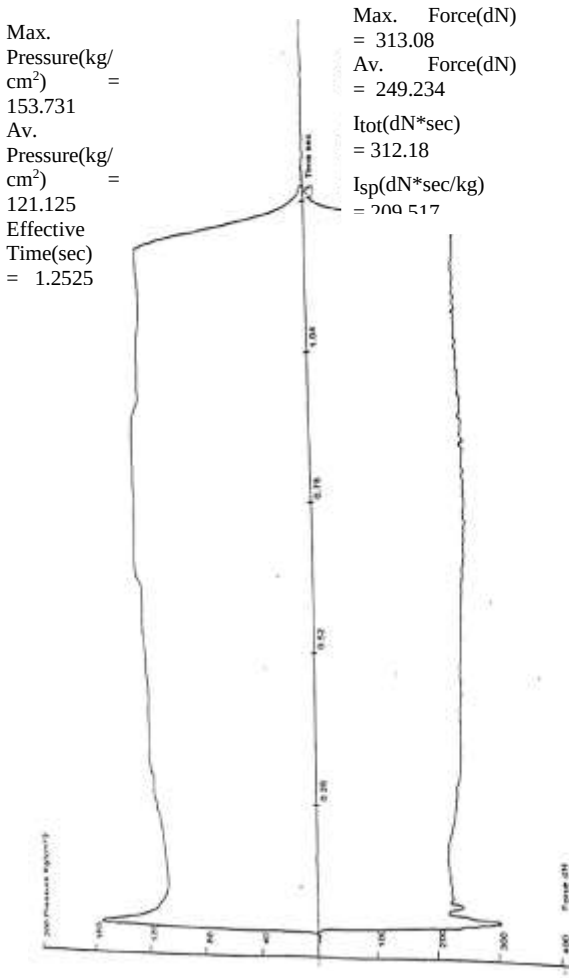

Fig. 5: Pressure-Time and Thrust-Time Curves

The results of the (P - t) and (f-t) curves are given in Figure 5. The burning time of the rocket motor is about (1.2 s), the average thrust is (2548 N) and the average pressure is (82.97 bar).

5 Results and Discussions

Figure 6 gives the measured temperatures through gauge (No.1) from experimental running by sensors TC1, TC2, and TC3 in the convergent section for the (9 s) period. Sensor TC1 reads the maximum value of measured temperature, which is about (477.5 K) at (3.5 s). The sensors (TC2 and TC3) read maximum measured temperatures (390 K) at (4 s) from starting. Normally, TC1 is the more response and effect sensor by the heat transfer from the others due to their location at (8mm) from the hot surface. After (8 s) the reading gives that, the rod reached to steady temperature and their temperature decreased with time.

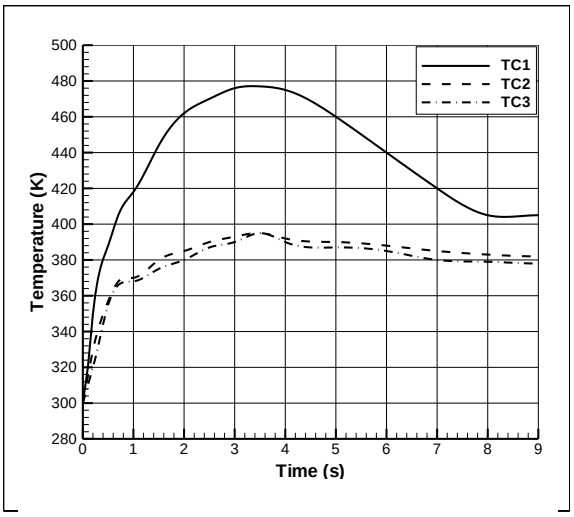

Fig. 6: Temperature measurement gradient along gauge No -1-

Figure 7 shows the reading of measured temperature by sensors TC1, TC2, and TC3 in the throat section from gauge (No.2) for the (9 s) period. (TC1) curve reaches a maximum value of measured temperature is about (637 K) at (3.6 s). (TC2) curve reaches a maximum value of measured temperature is about (500K) at (4.9 s), and the (TC3) curve reaches a maximum value of measured temperature is about (455 K) at (5.3 s). These differences in maximum reading temperature by the sensors come from the heat diffusion in material between the hot surface and the sensor locations. Normally the heat is transferred from one position to another when gradients in temperatures exist along the rod, thus causing a loss of energy inside the metal and the maximum temperature is reduced along the gauge.

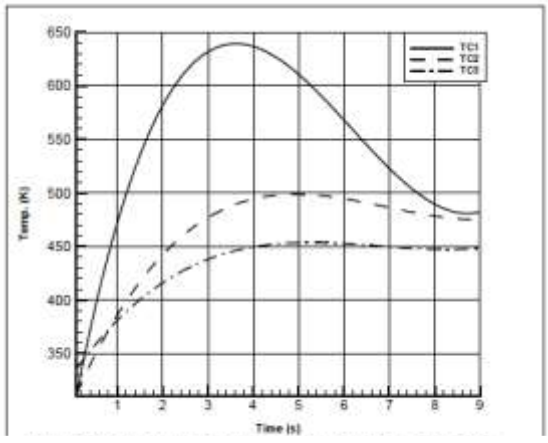

Fig.7 Temperature measurement gradient along gauge No -2-

Figure 8 shows the measured temperatures by sensors TC1, TC2, and TC3 in the divergent section by gauge (No.3). (TC1) measured transient temperature gradient higher than TC2 just to (1.3 s) where the cuts off the motor operation after this period the two curves are closely one to another with some differences in maximum temperature. This is because the distance between the two measured locations, which doesn't prevent reaching a maximum reading temperature is about (465 K) at the same time which is about (3.5 s) with differences between the two curves. The three above figures give differences in initial reading values between the curves in each figure, these are due to the temperature approximations by the polynomial function.

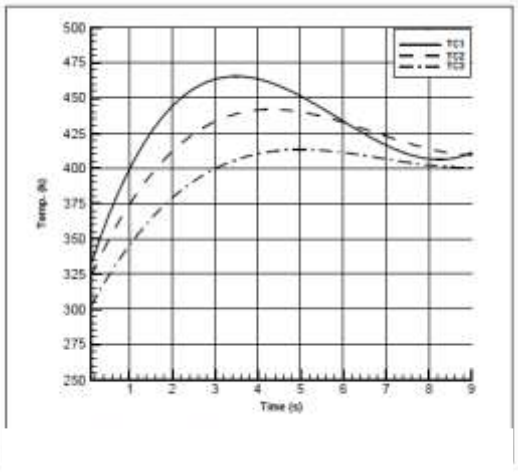

Fig. 8: Temperature measurement gradient along gauge No -3-.

Figure 9 shows the transient surface temperature predictions in convergent, throat, and divergent sections. The first curve is the surface temperature predictions at the convergent section, which indicate that the internal surface reaches a maximum temperature is about (480 K) at (3 s) from starting, i.e. the internal surface may receive heat from the internal environment through this period. The surface temperatures are decreased with time to reach a steady state after (8 s). The second curve is the surface temperature at the throat section which indicates that it is increased from the initial value is (300 K) to a maximum value is about (640 K) at (3.5 s), after that the surface temperature is decreased to a steady state at (8.5 s). The third curve gives the surface temperatures in the divergent section which are increased from (300 K) to the maximum value is about (462 K) at (3.5 s) also after this time the surface temperature is decreased to a steady state temperature as shown by the figure. The

differences between the throat and divergent curves indicate that the free-stream gas temperatures are decreased when moving from the throat section at Gauge No.2 to the divergent section at gauge No.3. This decrease in gas temperature coming from the heat losses to walls between the two locations of gauge and also due to expansion in the divergent region. No differences in time were appearing in curves to reach maximum surface temperatures. This justifies the accurate time constant calculation of thermocouples, it was very small and can be negligible.

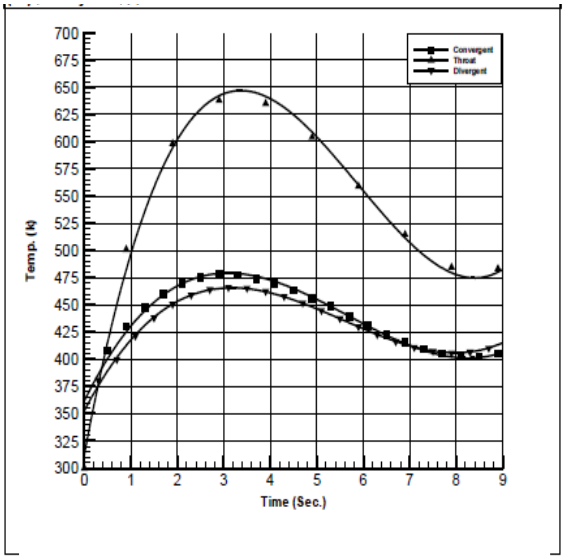

Fig. 9: Transient surface temperatures prediction.

Figure 10 shows the prediction of heat flux with time in the rocket motor nozzle with the application of equation (5). At the convergent section, the values of heat flux are changed from (0 to 4.6)*10^7 W/m^2 for (0.1 s). After this time the heat flux is decreased to the steady state value which is about 2*10^6 W/m^2. At the throat section, the heat flux is increased from zero to a maximum value of about (1.9*10^7) W/m^2 for (0.1 s) and then is decreased to the steady state value which is about 5*10^6 W/m^2 from (0.4 s). At the divergent section the heat flux is increased from zero to (9*10^6 W/m^2) for (0.2 s) and then decreased to steady state value which is about (2*10^6 W/m^2) from (0.4 s). The above heat flux predictions give that, at the beginning of the rocket motor starting the gases flow in the nozzle are in transient form starting until (0.4 s) due to the variable heat flux predictions. After (0.4 s) stable predictions of heat flux in convergent, throat and divergent sections as shown in figure. The results indicate that after (0.33 s) the heat flux in the throat section are more than the heat flux in convergent and divergent sections through the operation period because the throat section are exposed to high gas temperature and high velocity. This result justifies that, the throat region is exposed to maximum heat transfer in rocket motor nozzles.

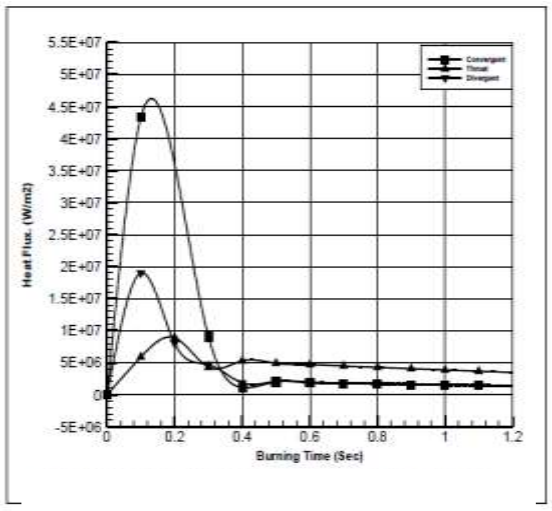

Fig. 10: Estimation heat flux along rocket motor nozzle.

6 Conclusions

The new iteration procedure and technique are capable of estimating the values of wall heat flux and surface temperatures from the measured temperature by Heat-Flux gauges. The estimation results indicate that the throat region is exposed to the maximum heat transfer with respect to other regions. The numerical approach is capable of handling the irregular behavior of the surface heat flux. The new experimental technique operates with a high-pressure environment which is about (82.97 bar) to estimate the surface temperatures and heat flux compared with the technique used with liquid RM given by [17] which operates with a pressure of (5bars).

References:

[1] Liebert C.H., "An Investigation of the Compatibility of Radiation and Convection Heat Flux Measurements", *NASA – TM – 107205*, 1996.

[2] W. Shoubin, Z. Li, S. Xiaogang, and J. Huangchao, "Inversion of thermal conductivity in two-dimensional unsteady-state heat transfer system based on boundary element method and decentralized fuzzy inference", *Complexity*, vol. 2018, Article ID 8783946, pp.1-9, 2018.

[3] S. Wang, Y. Deng and X. Sun, "Solving of two-dimensional unsteady inverse heat conduction problems based on boundary element method and sequential function specification method", *Complexity*, vol. 2018, Article ID 6741632, 2018, 11 pages.

[4] S.Wang, H. Jia, X. Sun, and L. Zhang, "Research on the recognition algorithm concerning geometric boundary regarding heat conduction based on BEM and CG", *Mathematical Problems in Engineering*, vol. 2018, Article ID 3723949, pp. 1-13, 2018.

[5] S. Wang, L. Zhang, X. Sun et al., "Solution to two-dimensional steady inverse heat transfer problems with interior heat source based on the conjugate gradient method", *Mathematical Problems in Engineering*, vol. 2017, Article ID 2861342, pp. 1-9, 2017.

[6] S. Wang, H. Jia, X. Sun et al., "Two-dimensional steady state boundary shape inversion of CGM-SPSO algorithm on temperature information", *Advances in Materials Science and Engineering*, vol. 2017, Article ID 2461498, pp.1-12,2017.

[7] C. Fieberg, R. Kneer, "Determination of thermal contact resistance from transient temperature measurements", *International Journal of Heat and Mass Transfer*, Vol.51, pp 1017–1023, 2008.

[8] M. S. Dargusch1, A. Hamasaiid1 et al., "An Inverse Model to Determine the Heat Transfer Coefficient and its Evolution with Time during Solidification of Light Alloys", *International Journal of Nonlinear Sciences and Numerical Simulation*, Vol.9, No.3, pp 275-282, 2008.

[9] Hua Liu, Xinlin Xia et al., "Experimental investigations on temperature-dependent effective thermal conductivity of nanoporous silica aerogel composite", *Experimental Thermal and Fluid Science*, Vol.84, pp 67-77, 2017.

[10] Shoubin Wang and Rui Ni, "Solving of Two-Dimensional Unsteady-State Heat-Transfer Inverse Problem Using Finite Difference Method and Model Prediction Control Method", *Hindawi Complexity*, Vol. 2019,Article ID 7432138, pp.1-12, 2019.

[11] Mehta R.C., "Estimation of Heat – Transfer Coefficient in a Rocket Nozzle", *AIAA Journal*, Vol.19, No.8, 1981, pp 1085-1086,.

[12] Anderson D.A., "*Computational Fluid Dynamics*", McGraw-Hill Inc., 1995.

[13] Nogier J.P , *"Methodes de Calcul Numerique"*, ISBN 2-225-78980-0, Masson, Paris, 1983.

[14] Bolton W. , *"Measurement and Instrumentation System*", ISBN 0 7506 3114 7, British Library, London, 1996.

[15] *"Manual on the Use of Thermocouples in Temperatures Measurements*", ASTM Publications, 1971.

[16] Marvian D.S. and Isoidore W., "Experimental Determination of Time Constant and Nusselt Numbers for Bare-Wire Thermocouples in High-Velocity air Streams and Analytic Approximation of Conduction and Radiation Errors", *NASA- TN 2599*, Washington, January, 1952.

[17] Sternfelf H. J. and Reinkenhof J., "Technique for Determining Local Heat – Transfer Coefficients", *AIAA Journal*, Vol.15, No.1, 1977, pp 105-109.